The Meteoritical Society

Meteoritics & Planetary Science 46, Nr 8, 1217–1225 (2011)
doi: 10.1111/j.1945-5100.2011.01226.x

A numerical comparison with the Ceplecha analytical meteoroid orbit determination method

David L. CLARK* and Paul A. WIEGERT

Department of Physics and Astronomy, University of Western Ontario, London, ON N6A 5B8, Canada
*Corresponding author. E-mail: dclark56@uwo.ca

(Received 16 January 2011; revision accepted 11 May 2011)

Abstract–Analytic methods by Ceplecha have long been used for the determination of meteoroid heliocentric orbits. These methods include both the derivation of an initial atmospheric contact position and velocity state, and the calculation of an orbit at infinity based on zenithal attraction assumptions. Herein, we describe a numerical integration-based verification for a portion of the Ceplecha methods, a verification driven by the need for an accurate meteoroid ephemeris in the hours before atmospheric contact. We show a close correspondence in analytic and numerical results, with a previously undocumented minor correction to a meteoroid's longitude of the ascending node.

INTRODUCTION

In 2007, the Fireball Retrieval on Survey Telescopic Image project (FROSTI) (Clark 2010) was initiated to locate meteoroids on pre-existing sky survey images. That is, we take a set of observed fireballs and ask whether or not the objects in question were serendipitously observed by one of the large telescopes. If a search of the telescope digital archive turns up images of the correct portion of the sky at the correct time, we examine these images further to determine whether or not the meteoroid was inadvertently imaged in the days or hours before impact.

An important aspect of this project is the ability to accurately model the location of a meteoroid at specific epochs in the hours before atmospheric contact. Ceplecha (1987) describes the complete process for deriving a heliocentric meteoroid orbit at infinity from multistation photographic records of a meteor event. We use the term "orbit at infinity" for expediency to refer to the orbit of a meteoroid before it is appreciably perturbed by the Earth. Implementations of these methods continue to be used in video-based meteor observing systems, both in the determination of contact position and velocity state of a meteoroid, and the derivation of a heliocentric orbit from that state. However, neither the instantaneous orbital elements at the time of contact, nor the computed orbit at infinity, may be used to provide an accurate position of the object at all points in time before contact. During this time, the Earth's gravity continuously perturbs the meteoroids orbit as it approaches the Earth. Therefore, it was decided to implement a gravitational integrator to model the trajectory of a meteoroid on Earth approach. The integrator steps back in time in increasing step sizes, beginning with the atmospheric contact time, and ending at an arbitrary 2 months before contact. At this point the object's heliocentric orbit can be assumed to be very near the orbit at infinity. We compare the differences between the orbit at infinity obtained by this numerical method and that obtained by using the analytical method of Ceplecha (1987).

Published data on meteor events typically include both the contact state and the computed orbital elements. The form and reference frames of the contact state vary by publication. The object contact position is typically provided in geocentric or geographic longitude, latitude, and height, but may be provided in geocentric rectangular form. The object's contact velocity vector is often described in an apparent J2000 equatorial radiant with an absolute velocity magnitude, but again may be provided in a geocentric rectangular vector form. In all cases encountered so far, the provided state needed to be adjusted to account for the Earth's position and its rotational and orbital motion. The publication of contact state and elements fortuitously permits the verification of both the gravitational integration approach and the

Ceplecha analytical orbit determination method. The altitude at which meteors are first observed varies from roughly 80–120 km (Ceplecha et al. 1998), the altitude being dependent on meteor characteristics, atmospheric conditions, the location of the observer, and the characteristics of the instrumentation used. It is assumed that the path of a meteoroid during initial atmospheric contact is dominated by the original orbital path and perturbation due to Earth's gravity, and not by interaction with the upper atmosphere. Therefore, the choice of contact position along the object path should not significantly alter the resulting orbit at infinity derived by either the analytic or numerical methods.

The data used in this report are two collections of 10 fireball events from the European Network. The first collection consists of the 10 largest mass events published in Spurný (1997). The second collection was provided by Spurný in private correspondence (Spurný personal communication), including previously published orbits: EN060402 Neuschwanstein (Spurný et al. 2002), EN171101 Tur'yi Remety (Spurný and Porubčan 2002), EN280506 Legnica (Spurný et al. 2007), and EN310800 Vimperk (Spurný and Borovička 2001).

FIREBALL DATA

The data of interest extracted from Spurný (1997, personal communication) that define the atmospheric contact state of an event are: h_B, λ_B, φ_B, the geographic altitude, longitude, and latitude of the beginning of the detected fireball trail; α_R, δ_R, the J2000 apparent right ascension and declination of the fireball radiant; and v_∞, the speed of the object with respect to the observer at contact. The calculated heliocentric orbits are expressed with the J2000 orbital elements: a, semi-major axis; e, eccentricity; i, inclination; Ω, longitude of the ascending node; and ω, argument of perihelion. In the Spurný (1997) paper, means and standard deviations are provided for all contact state measures including the epoch of the event, and for all calculated orbital elements. In Spurný (personal communication), the uncertainties in epoch and position are not provided. Spurný states that these uncertainties are accounted for in the uncertainties in the radiant and velocity. The relevant data from the two Spurný collections are listed in Tables 1 and 2.

METHOD

The numerical determination of a meteoroid's orbit at infinity involves calculating a collection of possible heliocentric position and velocity states at contact, gravitationally integrating these states back over time, and performing a statistical summarization over the sets of orbital elements calculated from the states at the end of the integration. The heliocentric contact state of an object is represented as a cloud of 10,000 probability members, each member having geographic position (λ_B, φ_B, h_B) and a velocity vector represented by radiant (α_R, δ_R) and velocity v_∞, all at an epoch t, where each of these values (including the epoch) are generated from a Gaussian distribution over the reported means and standard deviations. If a value's standard deviation was not provided, the reported value was used as the mean with a standard deviation of 0. Each probability cloud member's position-velocity contact state is converted to heliocentric coordinates (x_H, y_H, z_H) and (v_{xH}, v_{yH}, v_{zH}), in preparation for integration of each member, as follows:

- The member's geocentric coordinates centered on Greenwich (x_G, y_G, z_G) are calculated using the WGS84 theory (Defense Mapping Agency, 1996).
- The mean rotation of the Earth θ is calculated using the methods of Meeus (1991) Chapter 11.
- The apparent sidereal rotation of the Earth θ' is calculated from θ as described in Chapters 11 and 21 of Meeus (1991). This involves the calculation of the mean obliquity of the ecliptic ε_0, the nutation in longitude $\Delta\Psi$, and the nutation in obliquity $\Delta\varepsilon$. The calculations of nutation and obliquity require that the time of the event be expressed in Dynamical Time (TD), not universal time (UT). This difference in these timeframes is taken from a table of adjustments available on the US Naval Observatory web site (USNO, 2010).
- The geocentric position (x_G, y_G, z_G) is rotated by θ' giving the Earth-centered equatorial coordinates with respect to the equinox of the date (x_E, y_E, z_E).
- (x_E, y_E, z_E) are converted to equinox J2000 (x_{EJ}, y_{EJ}, z_{EJ}) by converting to spherical coordinates (α_E, δ_E, r_E), precessing to J2000 by the methods of Meeus (1991, chapter 20), and converting back to rectangular coordinates. The J2000 right ascension α_E is retained for later use.
- The apparent contact velocity of the probability cloud member equinox J2000 (v_{xoJ}, v_{yoJ}, v_{zoJ}) is calculated directly from α_R, δ_R, and negated v_∞.
- The velocity due to the rotation of the Earth (v_{xRot}, v_{yRot}, v_{zRot}) is the tangent vector at the probability cloud member's Earth-centered position expressed in equatorial coordinates for the epoch of the date. The magnitude v_{ROT} of the velocity is taken from a complete rotation of the earth at the member's distance and declination. Care must be taken that a sidereal adjustment be made if the Earth's rotation period is expressed in solar time units. v_{xRot} and v_{yRot} are then calculated from v_{ROT} and α_E; v_{zRot} is 0.

Table 1. The 10 largest mass events selected from Spurný (1997).

Fireball No.	EN220293	EN070893	EN150294	EN070594	EN250594	EN220495A	EN241095B	EN251095A	EN231195	EN150396
Name	Meuse	Polnã	Dresden	Leszno	Ulm	Koutim	Odra	Tisza	J. Hradec	Dobříš II
Epoch	1993/02/22	1993/08/07	1994/02/15	1994/05/07	1994/05/25	1995/04/22	1995/10/24	1995/10/25	1995/11/23	1996/03/15
	22:12:45 ± 2 s	21:08:15 ± 15 s	23:06:23 ± 5 s	20:03:41 ± 1 s	21:28 ± 1 m	22:28:40 s ± 3 s	21:01 ± 1 m	02:25:53 ± 1 s	01:29 ± 1 m	19:24:36 ± 9 s
h_B (km)	77.3 ± 0.2	77.194 ± 0.003	81.64 ± 0.06	63.56 ± 0.04	80.6 ± 0.2	89.01 ± 0.03	71.9 ± 0.3	80.54 ± 0.10	93.79 ± 0.05	73.6 ± 0.9
λ_B°	5.503 ± 0.004	15.7937 ± 0.0001	14.1013 ± 0.0010	15.4953 ± 0.0002	9.012 ± 0.003	15.3106 ± 0.0005	17.168 ± 0.009	20.197 ± 0.002	14.1185 ± 0.0008	13.392 ± 0.013
φ_B°	49.535 ± 0.003	49.4174 ± 0.0001	51.3766 ± 0.0004	51.4614 ± 0.0004	48.708 ± 0.002	49.2208 ± 0.0002	51.965 ± 0.005	47.4624 ± 0.0012	49.2463 ± 0.0006	50.07 ± 0.02
α_R°	189.4 ± 0.2	278.67 ± 0.06	273.96 ± 0.03	113.3 ± 0.3	102.9 ± 0.3	215.36 ± 0.02	47.8 ± 0.3	57.0 ± 0.2	41.6 ± 0.3	25.7 ± 0.7
δ_R°	43.3 ± 0.3	36.01 ± 0.014	69.41 ± 0.02	8.5 ± 0.3	29.35 ± 0.07	−6.397 ± 0.009	66.17 ± 0.02	16.87 ± 0.10	40.09 ± 0.02	36.6 ± 1.3
v_∞ (km s^{-1})	26.74 ± 0.09	17.61 ± 0.02	23.849 ± 0.008	14.01 ± 0.02	15.70 ± 0.03	27.534 ± 0.006	33.17 ± 0.10	29.23 ± 0.04	22.200 ± 0.013	19.1 ± 0.2
a (AU)	1.50 ± 0.02	2.003 ± 0.006	2.338 ± 0.003	2.10 ± 0.02	2.04 ± 0.02	2.374 ± 0.004	1.327 ± 0.011	1.077 ± 0.009	3.39 ± 0.05	7.2 ± 1.1
e	0.567 ± 0.004	0.5162 ± 0.0013	0.5783 ± 0.0006	0.532 ± 0.004	0.560 ± 0.003	0.7878 ± 0.0003	0.571 ± 0.002	0.8067 ± 0.0010	0.779 ± 0.003	0.88 ± 0.02
i°	32.6 ± 0.2	18.90 ± 0.03	33.841 ± 0.012	6.91 ± 0.07	2.50 ± 0.04	4.119 ± 0.012	52.8 ± 0.2	6.2 ± 0.2	11.99 ± 0.02	8.3 ± 0.5
Ω°	334.4071 ± 0.0001	135.4415 ± 0.0002	327.1296 ± 0.0001	227.1096 ± 0.0001	244.5262 ± 0.0007	32.3858 ± 0.0001	211.0381 ± 0.0007	31.2595 ± 0.0001	240.3362 ± 0.0007	355.5530 ± 0.0001
ω°	266.9 ± 0.8	209.52 ± 0.07	173.90 ± 0.02	338.2 ± 0.2	313.1 ± 0.3	277.58 ± 0.05	280.2 ± 0.4	140.4 ± 0.4	243.3 ± 0.3	141.2 ± 0.9

Table 2. Ten more recent events from Spurný (personal communication).

Fireball No.	EN210199	EN310800	EN171101	EN060402	EN170702	EN290903	EN280506	EN231006	EN040207	EN300807
Name		Vimperk	Tur'yi Remety	Neuschwanstein			Legnica			
Epoch	1999/01/21	2000/08/31	2001/11/17	2002/04/06	2002/07/17	2003/09/29	2006/05/28	2006/10/23	2007/02/04	2007/08/30
	18:05:00	22:51:56.0	16:52:46.7	20:20:17.7	23:51:01.5	01:20:12.6	23:16:42.0	23:38:06.0	22:59:15.0	22:17:43.1
h_B (km)	80.38	81.82	81.37	84.95	87.14	89.39	88.04	78.05	86.1	72.91
λ_B°	18.79	14.0843	23.7428	11.5524	17.3698	18.2982	15.8335	18.6956	16.9313	18.2469
φ_B°	50.14	49.5048	48.9196	47.3039	49.8902	49.6852	50.4327	48.2487	48.7966	48.8046
α_R°	36.1616 ± 0.8544	91.3351 ± 0.0740	43.1453 ± 0.1283	190.6207 ± 0.0147	311.563 ± 0.0511	3.5075 ± 0.0324	243.4151 ± 0.0133	36.6319 ± 0.0442	134.8135 ± 0.0173	299.7257 ± 0.0944
δ_R°	79.4351 ± 0.1570	76.5341 ± 0.0290	37.5387 ± 0.2537	21.9712 ± 0.0134	6.6323 ± 0.0507	13.7641 ± 0.0314	-7.0082 ± 0.0176	16.1281 ± 0.0251	31.267 ± 0.0209	18.2077 ± 0.0896
v_∞ (km s^{-1})	16.3389 ± 0.0339	14.9150 ± 0.0041	18.4825 ± 0.0138	20.9460 ± 0.0400	20.7277 ± 0.0088	23.1116 ± 0.0064	17.5755 ± 0.0050	28.7781 ± 0.0230	22.0526 ± 0.0307	16.6560 ± 0.0090
a (AU)	1.73 ± 0.011	0.7969 ± 0.0002	1.326 ± 0.004	2.4 ± 0.02	1.0002 ± 0.0011	2.019 ± 0.004	1.3936 ± 0.0006	2.39 ± 0.01	2.34 ± 0.01	2.529 ± 0.009
e	0.44 ± 0.003	0.2958 ± 0.0003	0.4844 ± 0.0011	0.67 ± 0.002	0.5343 ± 0.0004	0.7027 ± 0.0004	0.4691 ± 0.0003	0.8226 ± 0.0007	0.6997 ± 0.0015	0.629 ± 0.001
i°	17.56 ± 0.06	16.74 ± 0.02	7.41 ± 0.13	11.41 ± 0.03	14.12 ± 0.04	6.48 ± 0.02	2.55 ± 0.01	0.53 ± 0.03	6.92 ± 0.02	11.06 ± 0.03
Ω°	301.2713 ± 0.0007	158.81694 ± 0.00001	235.39271 ± 0.00002	16.82664 ± 0.00001	115.18836 ± 0.00001	185.45401 ± 0.00001	67.41318 ± 0.00007	210.281 ± 0.003	315.64715 ± 0.00001	157.06046 ± 0.00001
ω°	198 ± 0.2	19.13 ± 0.03	266.8 ± 0.2	241.2 ± 0.06	303.74 ± 0.11	268.39 ± 0.07	261.1 ± 0.03	285.71 ± 0.09	252.33 ± 0.03	215.25 ± 0.11

- (v_{xRot}, v_{yRot}, v_{zRot}) are converted to equinox J2000 (v_{xRotJ}, v_{yRotJ}, v_{zRotJ}) as with the geocentric position above.
- The Earth-centered equatorial J2000 velocity (v_{xEJ}, v_{yEJ}, v_{zEJ}) is the sum of (v_{xoJ}, v_{yoJ}, v_{zoJ}) and (v_{xRotJ}, v_{yRotJ}, v_{zRotJ}).
- The Earth-centered equatorial J2000 position (x_{EJ}, y_{EJ}, z_{EJ}) and velocity (v_{xEJ}, v_{yEJ}, v_{zEJ}) are converted to heliocentric coordinates (x_{EH}, y_{EH}, z_{EH}) and (v_{xEH}, v_{yEH}, v_{zEH}) by adding the Earth's position at the epoch using the JPL Horizons DE405 ephemeris (Markwardt 2010). The epoch must be expressed in Terrestrial Time (TT), equivalent to TD as calculated above.
- These equatorial coordinates are converted to heliocentric ecliptical coordinates (x_H, y_H, z_H) and (v_{xH}, v_{yH}, v_{zH}) by converting to spherical coordinates, converting to ecliptical coordinates as in Meeus (1991, chapter 12), and converting back to rectangular coordinates. These calculations again require ε_0 and $\Delta\varepsilon$ as calculated above.

Not wanting to re-invent the wheel in the field of numerical integrators, and understanding that this application did not require optimizations for performance, an existing C-language implementation of the RADAU-15 was adapted for this project. RADAU-15 is a 15th-order differential equation integrator documented in Everhart (1985). The RADAU family of integrators is characterized by the use of Gauss-Radau spacings for sequence substeps. The initial implementation of the RADAU integrator was tested by integrating the major objects of the solar system over 100 years, and comparing the results to the JPL DE405 ephemerides. The results of this comparison were deemed acceptable for the purposes of this project (e.g., an 8 arc-second difference in solar longitude and an oscillating .0000004 AU error in solar distance for Earth after 100 years). This test required the implementation of relativistic adjustments, a refinement not required for the integration of meteoroid objects on Earth approach.

To reduce the potential for overly large time-steps introducing errors in the integration, four integration runs were performed on each of the 10,000 object probability cloud members representing each fireball event: the 30 s before contact at 1/30 s time steps, the remainder of the first 5 min at 1 s time steps, the remainder of the first day at 1 min time steps, and the remainder of the first 2 months at 1 h time steps. The final positions in heliocentric rectangular coordinates at 2 months before contact are the only results of interest for this article. However, the heliocentric position-velocity state at each time step was stored to support the visualizations of probability cloud evolution over time, and to provide visual clues of the position of the object in any discovered sky survey images. Approximately 4,000 time steps are stored for each of the 10,000 members of each event, resulting in approximately 2 gigabytes of ephemeris data per event.

The above integration results in a position-velocity state (x_{H0}, y_{H0}, z_{H0}, v_{xH0}, v_{yH0}, v_{zH0}) derived from each calculated probability cloud member contact state (x_H, y_H, z_H, v_{xH}, v_{yH}, v_{zH}). Each instance of (x_{H0}, y_{H0}, z_{H0}, v_{xH0}, v_{yH0}, v_{zH0}) is converted to orbital elements (a_0, e_0, i_0, Ω_0, ω_0) using standard techniques. The mean and standard deviation of each orbital element is calculated across the 10,000 members arriving at a calculated (a, e, i, Ω, ω) with uncertainties for each meteor event. These orbital elements and uncertainties are compared to the published values for the orbits at infinity. In should be noted that there is high covariance among the orbital elements, so a probability cloud generated from both an event's calculated and published orbital elements and uncertainties exceeds the size of the cloud represented by the set of integrated heliocentric states.

An analysis was performed on the Spurný (1997, personal communication) event integrations to measure the validity of the arbitrary 2-month integration duration decision. Using the definition of convergence to n digits being the point at which all orbital elements measured in AU or degrees cease to vary by more than 0.5×10^{-n}/h, convergence to four digits occurred from 1.2 to 8.0 days into the integrations. Convergence to five digits occurred as quickly as 4.0 days, but in many cases did not occur at all within the 2-month duration. This failure to converge is consistent with precession and other perturbation effects. One could conclude that the 2-month duration could be relaxed somewhat to arrive at a meaningful precision. Errors due to the integrator and the choice of integration steps were measured by forward integrating the meteoroids of the two Spurny collections, starting at the calculated position-velocity states 2 months before contact, and ending at the time of contact. The largest distance between the original and integrated contact points was 22 m., and the greatest difference in contact speed was 0.015 m/s.

RESULTS AND ANALYSIS

Tables 3 and 4 show the comparison of integration derived orbit elements and published analytically derived results for the Spurný (1997, personal communication) event collections respectively. Orbital elements are presented to a constant number of decimal points for easier comparison and readability.

Table 3 and 4 demonstrate for the most part a good correspondence between published and integrated orbital elements, thereby supporting the Ceplecha analytic

Table 3. Comparison of integrated orbital elements to analytically derived results from Spurný (1997).

Event	Source	a	e	i	Ω	ω
EN070594	Integrated	2.1070 ± 0.0172	0.5328 ± 0.0037	6.8955 ± 0.0858	227.1324 ± 0.0004[a]	338.2586 ± 0.2567
Leszno	Published	2.1000 ± 0.0200	0.5320 ± 0.0040	6.9100 ± 0.0700	227.1096 ± 0.0001[b]	338.2000 ± 0.2000
	Delta	0.0070, −0.0028	0.0008, −0.0003	−0.0145, 0.0158	0.0228, 0.0003	0.0586, 0.0567
EN070893	Integrated	2.0050 ± 0.0282	0.5165 ± 0.0070	18.9062 ± 0.2539	135.4615 ± 0.0004[a]	209.5241 ± 0.0707
Polnã	Published	2.0030 ± 0.0060	0.5162 ± 0.0013	18.9000 ± 0.0300	135.4415 ± 0.0002[b]	209.5200 ± 0.0700
	Delta	0.0020, 0.0222	0.0003, 0.0057	0.0062, 0.2239	0.0200, 0.0002	0.0041, 0.0007
EN150294	Integrated	2.3391 ± 0.0133	0.5785 ± 0.0024	33.8456 ± 0.0346	327.1357 ± 0.0000[a]	173.9192 ± 0.1767
Dresden	Published	2.3380 ± 0.0030	0.5783 ± 0.0006	33.8410 ± 0.0120	327.1296 ± 0.0001[b]	173.9000 ± 0.0200
	Delta	0.0011, 0.0103	0.0002, 0.0018	0.0046, 0.0226	0.0061, −0.0001	0.0192, 0.1567
EN150396	Integrated	7.5504 ± 1.4374	0.8781 ± 0.0206	8.3212 ± 0.5063	355.5682 ± 0.0007[a]	141.1807 ± 0.9414
Dobríš II	Published	7.2000 ± 1.1000	0.8800 ± 0.0200	8.3000 ± 0.5000	355.5530 ± 0.0001[b]	141.2000 ± 0.9000
	Delta	0.3504, 0.3374	−0.0019, 0.0006	0.0212, 0.0063	0.0152, 0.0006	−0.0193, 0.0414
EN220293	Integrated	1.5065 ± 0.0187	0.5681 ± 0.0037	32.5932 ± 0.1548	334.4101 ± 0.0000[a]	266.8750 ± 0.8424
Meuse	Published	1.5000 ± 0.0200	0.5670 ± 0.0040	32.6000 ± 0.2000	334.4071 ± 0.0001[b]	266.9000 ± 0.8000
	Delta	0.0065, −0.0013	0.0011, −0.0003	−0.0068, −0.0452	0.0030, −0.0001	−0.0250, 0.0424
EN220495A	Integrated	2.3880 ± 0.0104[a]	0.7886 ± 0.0008[a]	4.1331 ± 0.0464[a]	32.4131 ± 0.0002[a]	277.3980 ± 0.0773[a]
Koutim	Published	2.3740 ± 0.0040[b]	0.7878 ± 0.0003	4.1190 ± 0.0120	32.3858 ± 0.0001[b]	277.5800 ± 0.0500[b]
	Delta	0.0140, 0.0064	0.0008, 0.0005	0.0141, 0.0344	0.0273, 0.0001	−0.1820, 0.0273
EN231195	Integrated	3.4417 ± 0.1152[a]	0.7814 ± 0.0066	11.9165 ± 0.5939[a]	240.3475 ± 0.0002[a]	242.8845 ± 1.9508[a]
J. Hradec	Published	3.3900 ± 0.0500	0.7790 ± 0.0030	11.9900 ± 0.0200	240.3362 ± 0.0007[b]	243.3000 ± 0.3000
	Delta	0.0517, 0.0652	0.0024, 0.0036	−0.0735, 0.5739	0.0113, −0.0005	−0.4155, 1.6508
EN241095B	Integrated	1.3083 ± 0.0849[a]	0.5670 ± 0.0192[a]	52.7780 ± 0.5534	211.0406 ± 0.0006[a]	281.3270 ± 4.1334[a]
Odra	Published	1.3270 ± 0.0110	0.5710 ± 0.0020	52.8000 ± 0.2000	211.0381 ± 0.0007[b]	280.2000 ± 0.4000
	Delta	−0.0187, 0.0739	−0.0040, 0.0172	−0.0220, 0.3534	0.0025, −0.0001	1.1270, 3.7334
EN250594	Integrated	2.0179 ± 0.1131[a]	0.5558 ± 0.0215[a]	2.5316 ± 0.7539	244.4786 ± 0.0214[a]	312.1663 ± 1.7810[a]
Ulm	Published	2.0400 ± 0.0200	0.5600 ± 0.0030	2.5000 ± 0.0400	244.5262 ± 0.0007[b]	313.1000 ± 0.3000
	Delta	−0.0221, 0.0931	−0.0042, 0.0185	0.0316, 0.7139	−0.0476, 0.0207	−0.9337, 1.4810
EN251095A	Integrated	1.0778 ± 0.0068	0.8068 ± 0.0010	6.1380 ± 0.1704	31.2536 ± 0.0004[a]	140.4169 ± 0.3212
Tisza	Published	1.0770 ± 0.0090	0.8067 ± 0.0010	6.2000 ± 0.2000	31.2595 ± 0.0001[b]	140.4000 ± 0.4000
	Delta	0.0008, −0.0022	0.0001, 0.0000	−0.0620, −0.0296	−0.0059, 0.0003	0.0169, −0.0788

Note: Integrated and published orbital element means and standard deviations are expressed to a consistent number of decimal for readability and numerical comparison. The number of decimals does not reflect data precision.

[a]Instances where the integrated mean lies outside one standard deviation of the published result.

[b]Instances where the published mean lies outside one standard deviation of the integrated result.

Table 4. Comparison of integrated orbital elements to analytically derived results from Spurný (personal communication).

Event	Source	a	e	i	Ω	ω
EN040207	Integrated	2.3328 ± 0.0101	0.6990 ± 0.0014	6.9374 ± 0.0188	315.6638 ± 0.0000[a]	252.5122 ± 0.0302[a]
	Published	2.3400 ± 0.0100	0.6997 ± 0.0015	6.9200 ± 0.0200	315.6472 ± 0.0000[b]	252.3300 ± 0.0300[b]
	Delta	−0.0072, 0.0001	−0.0007, −0.0001	0.0174, −0.0012	0.0166, 0.0000	0.1822, 0.0002
EN060402	Integrated	2.4042 ± 0.0161	0.6702 ± 0.0023	11.4224 ± 0.0294	16.8393 ± 0.0001[a]	241.1837 ± 0.0350
Neuschwanstein	Published	2.4000 ± 0.0200	0.6700 ± 0.0020	11.4100 ± 0.0300	16.8266 ± 0.0000[b]	241.2000 ± 0.0600
	Delta	0.0042, −0.0039	0.0002, 0.0003	0.0124, −0.0006	0.0126, 0.0001	−0.0163, −0.0250
EN170702	Integrated	0.9997 ± 0.0011	0.5344 ± 0.0004	14.1301 ± 0.0380	115.2047 ± 0.0000[a]	303.7823 ± 0.1052
	Published	1.0002 ± 0.0011	0.5343 ± 0.0004	14.1200 ± 0.0400	115.1884 ± 0.0000[b]	303.7400 ± 0.1100
	Delta	−0.0005, 0.0000	0.0001, 0.0000	0.0101, −0.0020	0.0163, 0.0000	0.0423, −0.0048
EN171101	Integrated	1.3269 ± 0.0043	0.4845 ± 0.0011	7.4167 ± 0.1303	235.4202 ± 0.0003[a]	266.7861 ± 0.2457
Tur'yi Remety	Published	1.3260 ± 0.0040	0.4844 ± 0.0011	7.4100 ± 0.1300	235.3927 ± 0.0000[b]	266.8000 ± 0.2000
	Delta	0.0009, 0.0003	0.0001, 0.0000	0.0067, 0.0003	0.0274, 0.0003	−0.0139, 0.0457
EN210199	Integrated	1.7311 ± 0.0107	0.4400 ± 0.0034	17.5574 ± 0.0644	301.2945 ± 0.0002[a]	197.9989 ± 0.2095
	Published	1.7300 ± 0.0110	0.4400 ± 0.0030	17.5600 ± 0.0600	301.2713 ± 0.0007[b]	198.0000 ± 0.2000
	Delta	0.0011, −0.0003	0.0000, 0.0004	−0.0026, 0.0044	0.0232, −0.0005	−0.0011, 0.0095
EN231006	Integrated	2.3752 ± 0.0103[a]	0.8219 ± 0.0007[a]	0.5397 ± 0.0288	210.4349 ± 0.0053[a]	285.8073 ± 0.0887[a]
	Published	2.3900 ± 0.0100[b]	0.8226 ± 0.0007	0.5300 ± 0.0300	210.2810 ± 0.0030[b]	285.7100 ± 0.0900[b]
	Delta	−0.0148, 0.0003	−0.0007, 0.0000	0.0097, −0.0012	0.1539, 0.0023	0.0973, −0.0013
EN280506	Integrated	1.3927 ± 0.0006[a]	0.4694 ± 0.0002	2.6020 ± 0.0097[a]	67.4834 ± 0.0003[a]	261.1741 ± 0.0283[a]
Legnica	Published	1.3936 ± 0.0006[b]	0.4691 ± 0.0003[b]	2.5500 ± 0.0100[b]	67.4132 ± 0.0001[b]	261.1000 ± 0.0300[b]
	Delta	−0.0009, 0.0000	0.0003, −0.0001	0.0520, −0.0003	0.0703, 0.0002	0.0741, −0.0017
EN290903	Integrated	2.0139 ± 0.0035[a]	0.7024 ± 0.0004	6.4955 ± 0.0225	185.4732 ± 0.0000[a]	268.4863 ± 0.0652[a]
	Published	2.0190 ± 0.0040[b]	0.7027 ± 0.0004	6.4800 ± 0.0200	185.4540 ± 0.0000[b]	268.3900 ± 0.0700[b]
	Delta	−0.0051, −0.0005	−0.0003, 0.0000	0.0155, 0.0025	0.0192, 0.0000	0.0962, −0.0048
EN300807	Integrated	2.5231 ± 0.0094	0.6284 ± 0.0013	11.0862 ± 0.0332	157.0897 ± 0.0001[a]	215.3708 ± 0.1053[a]
	Published	2.5290 ± 0.0090	0.6290 ± 0.0010	11.0600 ± 0.0300	157.0605 ± 0.0000[b]	215.2500 ± 0.1100[b]
	Delta	−0.0059, 0.0004	−0.0006, 0.0003	0.0262, 0.0032	0.0293, 0.0001	0.1208, −0.0047
EN310800	Integrated	0.7965 ± 0.0002[a]	0.2962 ± 0.0003[a]	16.8169 ± 0.0152[a]	158.8592 ± 0.0001[a]	19.0122 ± 0.0255[a]
Vimperk	Published	0.7969 ± 0.0002[b]	0.2958 ± 0.0003[b]	16.7400 ± 0.0200[b]	158.8169 ± 0.0000[b]	19.1300 ± 0.0300[b]
	Delta	−0.0004, 0.0000	0.0004, 0.0000	0.0769, −0.0048	0.0423, 0.0001	−0.1178, −0.0045

Notes: Integrated and published orbital element means and standard deviations are expressed to a consistent number of decimal for readability and numerical comparison. The number of decimals does not reflect data precision.

[a]Instances where the integrated mean lies outside one standard deviation of the published result.

[b]Instances where the published mean lies outside one standard deviation of the integrated result.

Table 5. Analysis of integrated and published orbital elements.

Line	Statistic	a	e	i	Ω	ω
1	Cloud uncertainty = Largest mean value differences due to random number seeding of clouds	0.0001 AU	0.0000	0.0013 °	0.0001 °	0.0028 °
Analysis of 10 Spurný (1997) deltas in means and uncertainties (Delta = Integrated−Published)						
2	# events where delta of means is less than negative cloud uncertainty	2	3	5	2	5
3	# events where delta of means is greater than positive cloud uncertainty	8	7	5	8	5
4	# events where published uncertainties exceed integrated uncertainties	3	3	2	4	1
5	# events where integrated uncertainties exceed published uncertainties	7	7	8	6	9
6	# events where the integrated mean lies outside one standard deviation of the published result	4	3	2	10	4
7	# events where the published mean lies outside one standard deviation of the integrated result	1	0	0	10	1
Analysis of 10 Spurný (personal communication) deltas in means and uncertainties (Delta = Integrated−Published)						
8	# events where delta is less than negative cloud uncertainty	7	5	1	0	3
9	# events where delta is greater than positive cloud uncertainty	3	5	9	10	6
10	# events where published uncertainties exceed integrated uncertainties	5	5	6	1	7
11	# events where integrated uncertainties exceed published uncertainties	5	5	4	9	3
12	# events where the integrated mean lies outside one standard deviation of the published result	4	2	2	10	5
13	# events where the published mean lies outside one standard deviation of the integrated result	4	2	2	10	5

method. However, a deeper inspection reveals small discrepancies in means and uncertainties which bear mentioning. Because these discrepancies are relatively small, an understanding of uncertainties in the cloud integration method is important. Based on the testing of the RADAU integrator, it is believed the actual integration steps do not significantly add to uncertainties. However, the sampling of 10,000 probability cloud elements over seven dimensions (three position, three velocity, one time) does require attention. Multiple sets of 10,000-member event integrations were performed on the Spurný (personal communication) collection to determine the impact of differing random number seeds used for the initial geocentric state on the eventual orbital elements of probability cloud members. The largest difference in mean values of each orbital element are called "cloud uncertainties" for the purpose of this discussion, and are recorded in the first line of Table 5. Differences between published and integrated orbital elements that are smaller than the cloud uncertainties are ignored. The cloud uncertainties in fact have little impact on this analysis, as the majority of discrepancies noted exceed the cloud uncertainties.

Comparison of results begins with the comparison of the mean values of the orbital elements. Lines 2–3 and 8–9 of Table 5 enumerate the significant negative and positive deltas for the Spurný (1997, personal communication) event collections respectively. The Spurný (1997) data appear to indicate a systematic bias toward larger integrated a and Ω, with lesser significant or no bias on other elements, while the Spurný (personal communication) data indicate a bias toward larger integrated i and Ω. Note that these are statements on bias, not significance. The significance of the deltas depends on the uncertainties of the analytic methods. Lines 4–5 and 10–11 of Table 5 enumerate the numbers of events for which the published uncertainty range exceeds the integrated uncertainty range in size, and vice-versa. Spurný (1997) reports smaller uncertainty ranges for all elements than can be confirmed by the integration method. For the most part, Spurný (personal communication) is either equally or less aggressive on the uncertainty ranges than the integration method, with the sole exception of Ω. Lines 6–7 and 12–13 of Table 5 enumerate the cases where one method's results fall outside the uncertainty ranges of the other, and thus measures the significance of the deltas. The integrated results for Spurný (1997) fall reasonably well within the more aggressive published uncertainties, while the published results fall consistently within the integrated uncertainties for all elements but Ω. For Spurný (personal communication) and the similar uncertainty range sizes

for both the analytic and integration methods, we see good alignment of e and i, somewhat significant deltas in a and ω, and the significant delta in Ω as in the Spurný (1997) data. Positive deltas across the orbital elements appear more often than negative deltas, although with the exception of Ω, there does not appear to be consistent dominance in the sign of the deltas for any one element across both meteoroid collections.

The most obvious difference in published and integrated results is the consistent deltas in longitude of the ascending node Ω across all events in both data collections. The magnitudes of these deltas are not large, the largest being just over 0°.15 for the event EN231006. The significance of the deltas lies in the very tightly confined published uncertainties for Ω, consistently stated as $< 0°.001$ and often quoted as $\leq 0°.0001$. The source of the discrepancy lies in formula (48) of Section 11 of Ceplecha (1987), where Ω is directly derived from the longitude of the Sun, either as $\Omega = L_{SUN}$ or $\Omega = L_{SUN} - \pi$. This assumption does not take into account the perturbation of the meteoroid's orbit as it enters into Earth's gravity well. Formulas (38)–(40) of Ceplecha (1987) do account for the zenithal attraction of the radiant; however, this is only an adjustment to an observer-centered direction of motion. Formula (48) does not derive from (38)–(40), but instead reverts to an assumption that the post-perturbation heliocentric longitude of the Earth's location accurately reflects where the object would have passed through the ecliptic plane if the Earth were not nearby. For meteoroids on low inclination orbits (such as EN231006 at 0°.53), a small perturbation causing small inclination changes have substantial impact on the ascending node, the impact being dependent on cos i. This impact is difficult to illustrate with orbits of low inclination, but is more easily visualized with meteoroids with higher inclination orbits. The orbit Bunburra Rockhole meteoroid, documented in Bland et al. (2009) and in personal correspondence (Spurný personal communication), has a published orbit of $a = 0.851 \pm 0.002$ AU, $e = 0.245 \pm 0.003$, $i = 9°.07 \pm 0°.17$, $\Omega = 297°.59525 \pm 0°.00010$, $\omega = 209°.9 \pm 0°.2$ and an integrated orbit of $a = 0.851 \pm 0.002$ AU, $e = 0.246 \pm 0.003$, $i = 9°.11 \pm 0°.17$, $\Omega = 297°.696 \pm 0°.003$, $\omega = 209°.8 \pm 0.2$. Fig. 1 demonstrates the shift in Ω for Bunburra Rockhole, made more visually evident by its relative steep inclination. The dominance in positive deltas in Ω requires further analysis. A positive delta in Ω represents the meteoroid being drawn back toward the Earth, contacting the Earth at a lesser Ω than would have been the case if not perturbed. A cursory look at the geometry of the two negative delta Ω events shows EN250594 Ulm approaching the Earth sun-side, passing over the Earth before contacting on the night-side, and EN251095A Tisza's highly eccentric orbit carrying Tisza on a very steep night-side approach.

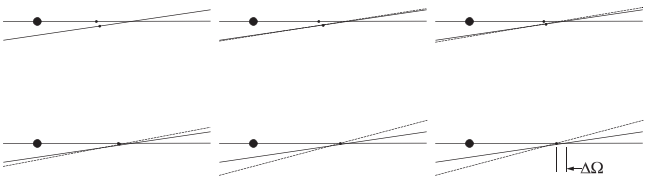

Fig. 1. The shift $\Delta\Omega$ of the ascending node Ω of the instantaneous orbit of the Bunburra Rockhole meteoroid. From left to right, top to bottom, the progress of the shift is shown, 4, 3, 2, and 1 h before contact, at contact, and at contact with the shift highlighted. The solid diagonal line represents the orbit at infinity. The dashed diagonal line represents the instantaneous orbit. The horizontal solid line represents the elliptic along which Ω is measured.

CONCLUSION

Numerical integrations of 20 meteoroid contact states yield consistent results with the analytic methods of Ceplecha (1987). The sole point of discrepancy is a small difference in the longitude of the ascending node Ω, this discrepancy being due to a failure to completely account for the impact of the Earth's gravity on the meteoroid path. The Ceplecha method assumes the heliocentric longitude of the Earth at contact reflects the pre-perturbation longitude of the node, which is not the case. The correction in Ω is small, 0.15 being the largest discrepancy yet encountered. In relation to the uncertain of the other orbital elements, this discrepancy is not overly significant, so the use of the existing analytic methods are likely sufficient for the categorization of meteoroid orbits. However, the very tight uncertainties often reported for Ω are far too aggressive, and should be minimally expanded to incorporate this discrepancy. If a highly accurate Ω is required, as would be the case for predicting the Earth's interaction with meteoroid streams, an analytic correction to the Ceplecha method should be developed.

Acknowledgments—The authors acknowledge Dr. Pavel Spurný (Astronomical Institute, Academy of Sciences of the Czech Republic) for his providing meteor observations and derived orbits, his many emails of support and clarifications, and his review of this article. We also thank Dr. Jérémie Vaubaillon (IMCCE–CALTECH) for his review. This work was supported in part by the Natural Sciences and Engineering Research Council of Canada and NASA's Meteoroid Environment Office.

Editorial Handling—Dr. Dina Prialnik

REFERENCES

Bland P. A., Spurný P., Towner M. C., Bevan A. W., Singleton A. T., Chesley S. R., Bottke W. F., Shrbenỳ L., Borovička J., McClafferty T., Vaughan D., Benedix G. K., Deacon G., and Hough R. M. 2009. A eucrite delivered from an Aten-type orbit: The last link in the chain from 4 Vesta to Earth. (abstract #1664). 40th Lunar and Planetary Science Conference, CD-ROM.

Ceplecha Z. 1987. Geometric, dynamic, orbital and photometric data on meteoroids from photographic fireball networks. *Astronomical Institutes of Czechoslovakia, Bulletin* 38): 222–234.

Ceplecha Z., Borovička J., Elford W. G., ReVelle D. O., Hawkes R. L., Porubčan V., and Šimek M. 1998. Meteor phenomena and bodies. *Space Science Reviews* 84:327–471.

Clark D. L. 2010. Searching for Fireball pre-detections in Sky Survey Images. M.Sc. thesis, University of Western Ontario, London, Ontario, Canada.

Defense Mapping Agency. 1996, Feb. *Technical Manual DMA TM 8358.1 - Datums, Ellipsoids, Grids, and Grid Reference Systems*. https://www1.nga.mil/ProductsServices/GeodesyGeophysics/Related%20Documents/TM8358_1.pdf, Accessed March 26, 2011, from National Geospatial-Intelligence Agency.

Everhart E. 1985. An efficient integrator that uses Gauss-Radau spacings. Dynamics of Comets: Their Origin and Evolution, Proceedings of IAU Colloq. 83, June 11–15 Rome, Italy, edited by Carus A. and Valsecchi G. B. 185p.

Markwardt C. B. 2010, Nov 18. *IDL JPL ephemeris and solar system timing*. http://cow.physics.wisc.edu/~craigm/idl/ephem.html, Accessed March 26, 2011, from Compact Objects at Wisconsin.

Meeus J. 1991. *Astronomical algorithms*. Richmond, VA: Willman-Bell, Inc. 477 p.

Spurný P. 1997. Exceptional fireballs photographed in central Europe during the period 1993–1996. *Planetary and Space Science* 45:541–555.

Spurný P. and Borovička J. 2001. EN310800 Vimperk fireball: Probable meteorite fall of an Aten type meteoroid. Proceedings of the Meteoroids 2001 Conference, 6–10, edited by Warmbein B. pp. 519–524.

Spurný P. and Porubčan V. 2002. The EN171101 bolide—The deepest ever photographed fireball. Proceedings of Asteroids, Comets, Meteors—2002. International Conference, 29 July–2 August 2002, edited by Warmbein B. pp. 269–272.

Spurný P., Heinlein D., and Oberst J. 2002. The atmospheric trajectory and heliocentric orbit of the Neuschwanstein meteorite fall on April 6, 2002. Proceedings of Asteroids, Comets, Meteors—ACM 2002. International Conference, 29 July–2 August 2002, Berlin, Germany, ESA Publications Division, edited by Warmbein B. pp. 137–140.

Spurný P., Borovička J., and Shrbený L. 2007. Automation of the Czech part of the European Fireball Network: equipment, methods and first results. Near Earth Objects, our Celestial Neighbors: Opportunity and Risk, Proceedings of IAU Symposium 236, edited by Valsecchi G. and Vokrouhlický D. pp. 121–130.

USNO. 2010. *Table of TAI-UTC differences*. Retrieved Mar 13, 2010, from US Naval Observatory: ftp://maia.usno.navy.mil/ser7/tai-utc.dat